Effect of Interfacial Phenomena on the Development of Particle Morphology in a Polymer Latex System

Yi-Cherng Chen, Victoria Dimonie, and Mohamed S. El-Aasser*

Emulsion Polymers Institute, Center for Polymer Science and Engineering and Department of Chemical Engineering, Lehigh University, Bethlehem, Pennsylvania 18015

Received March 8, 1990; Revised Manuscript Received January 30, 1991

ABSTRACT: Seeded batch emulsion polymerization was carried out at 70 °C using monodisperse polystyrene latex particles as seed and methyl methacrylate as second-stage monomer at different seed polymer/monomer weight ratios. The final composite latex particles were found to have a mixture of more than one nonuniform morphology. A thermodynamic analysis and a mathematical model were derived to describe the free energy changes corresponding to various possible thermodynamically unstable morphologies during the course of the seeded emulsion polymerization. On the basis of experimentally measured interfacial tensions, the relative stabilities of particle morphologies were calculated. The mechanism of changes in particle morphology during the polymerization is proposed. Thermodynamic analysis suggested that the observed mixed-particle morphology in the final latex is due to restricted chain mobility related to high internal viscosity during the final stage of the polymerization. When the composite latex samples were swollen with toluene, the particle morphology showed a tendency toward a thermodynamically more favorable morphology.

I. Introduction

Latex systems with well-designed particle morphology are necessary for advanced engineering plastics with high impact strength and improved toughening, optimum peel strength of adhesives, and many other high-value-added products in other application areas such as membrane separations and biotechnology. Composite latex particles of different morphological features[1-9] are usually prepared by seeded emulsion polymerization techniques where a second-stage monomer is polymerized in the presence of seed latex particles. Elucidation of the morphology of two-stage latex particles and the factors controlling it was the goal of many papers published in recent years; notably those of Sundberg et al.,[10] Dimonie et al.[11], Cho and Lee,[4] and Okubo et al.[8] These factors fall into two broad categories: thermodnyamics and kinetics. The thermodynamic factors detemine the equilibrium morphology of the final composite latex particle, and the kinetic factors determine the ease with which such thermodynamically favored morphology can be achieved. Studies are still lacking on the dynamic nature of the development of particle morphology and the morphological changes that take place during the polymerization reactions.

In terms of thermodynamics, Torza and Mason[12] pioneered the interfacial behavior of systems containing three mutually immiscible liquids. In this case the thermodynamics of the system were influential in determining the final morphology since the liquid phase was highly mobile. They examined the conditions necessary for a coacervate droplet (liquid 3) to engulf an initial droplet (liquid 1) when both are immersed in a continuous phase (liquid 2) by the spreading coefficient, S, which is defined as

$$S_i = \gamma_{jk} - (\gamma_{ij} + \gamma_{ik}) \quad (1)$$

If one assumes that the interfacial tension of liquid 1 against liquid 2 (γ_{12}) is greater than that of liquid 3 against liquid 2 (γ_{23}), only three possible sets of values for S exist. These correspond to the three different equilibrium configurations: complete engulfing (core–shell), partial engulfing (hemisphere), and nonengulfing (individual particle). Complete engulfing occurs only if $S_3 > 0$, $S_2 < 0$, and $S_1 < 0$. On the other hand, when $S_2 < 0$, $S_3 < 0$, and $S_1 < 0$, the partial engulfing was preferred. Torza and Mason demonstrated the general validity of their approach by making a number of interfacial tension measurements, calculating values of S, and then observing what occurred in an actual three-phase system. In most cases, predictions of engulfing based on S were satisfactory. This approach should be broadly applied in determining when the engulfing will occur in various encapsulation systems. Recently, Sundberg et al,[10] by applying Torza and Mason's approach, presented a thermodynamic analysis of the morphology of a system comprising a polymer encapsulating a relatively large size oil droplet in the micrometer range. Their analysis revealed that the interfacial tension of each phase is the key factor governing the type of microcapsules formed. Dimonie et al.[11] supported experimentally the hypothesis that, in addition to the viscosity of the polymerization locus (related to the chain mobility), the interfacial tension of the polymer phases is one of the main parameters controlling the particle morphology in a composite polymer latex system. In our previous work,[13] a thermodynamic analysis similar to that presented by Sundberg et al.[10] and a mathematical model were derived to describe the free energy changes corresponding to various composite latex particle morphologies (shown in Figure 1). The model was applied and verified for predicting the final morphology for particles in the submicron size range. The methodology involves consideration of the free energy changes for the following hypothetical pathways. In our previous paper we considered the initial state to consist of a pure polymer phase (seed particles of polymer 1) and another completely separated bulk phase of polymer 2 (postformed polymer). The volume ratio of polymer 2 to polymer 1 was assumed to be constant regardless of the present conversion. Since the emphasis of the current paper is on morphology development during the course of the polymerization, the original thermodynamic model was revised in order to reflect the reality of the latex system and to account for changes in the volume ratio of polymer 2 to polymer 1 that occur during the course of the polymerization. In the revised model, the initial state was considered to consist of a polymer phase 1 (seed particles of polymer 1 swollen by the second-stage monomer, i.e., monomer 2) suspended in water containing surfactant. The final state is one of the morphologies shown in Figure 1. Table I lists the revised equations describing the free energy changes corresponding to the various

0024-9297/91/2224-3779$02.50/0

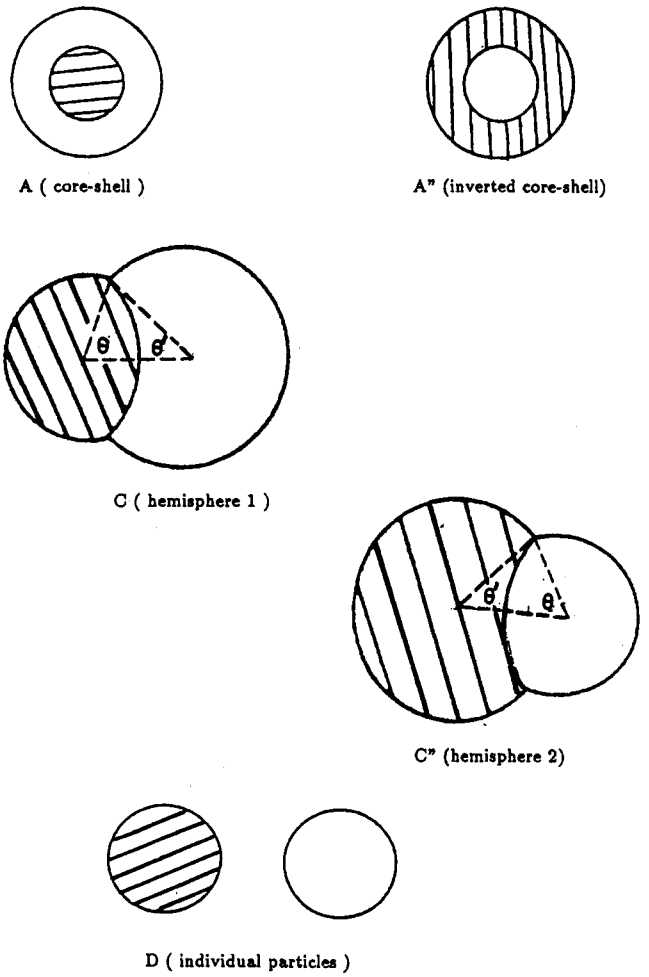

Figure 1. Various morphological structures of particles dispersed in water. ▨, polymer 1; □, polymer 2.

composite latex particle morphologies shown in Figure 1. The only contribution to the free energy change for this pathway is the creation of new interfaces and changes in the corresponding interfacial tensions. For latex particles dispersed in a continuous water phase, those interfaces include polymer phase 1/water, polymer phase 2/water, and polymer phase 1/polymer phase 2. Polymer phase 2 is polymer 2 (formed as a result of the polymerization of monomer 2 in the presence of polymer 1) swollen by its own monomer. The total concentration of monomer 2 is dependent on the conversion. The monomer distribution between polymer 1 and polymer 2 is assumed to be proportional to the weight fraction of each polymer. The total free energy change for all types of configurations shown in Figure 1 can be expressed as

$$\Delta G = \sum \gamma_{ij} A_{ij} - \gamma_o A_o \qquad (2)$$

where γ_{ij} is the interfacial tension between i and j and A_{ij} the corresponding interfacial area, γ_o is the interfacial tension of original polymer phase 1 (i.e., seed particles of polymer 1 swollen by monomer 2) suspended in water phase, and A_o is its interfacial area. The equations describing the free energy change for each case shown in Figure 1 are given in Table I. Equation 6 is related to the volume of polymer phase 1 in the composite particle at different conversions for case C in Figure 1. Equation 7 is based on the geometry of the triangle defined by angles θ and θ' in the same figure. Equations 6 and 7 are solved simultaneously in order to calculate θ' and R_2/R. These values are then used in eq 5 to calculate the change of surface energy per unit area for case C. A similar approach is used for hemisphere case C" employing eqs 8–10. The thermodynamically preferred morphology will be the one that has the minimum interfacial free energy change. On the basis of experimentally measured interfacial tensions, composite particle configurations prepared by seeded batch emulsion polymerization were predicted as a function of the polymer to monomer volume ratio. The morphology of the composite latex particle is examined by transmission electron microscopy after some preferential staining treatment. The observed morphology is compared to the predicted morphology. The kinetic parameters that influence the ease of chain mobility determine the extent to which thermodynamically predicted morphology is attained. The purpose of this paper is to report on the effect of interfacial phenomena on the development of particle morphology in a composite polymer latex system as a function of seed polymer/monomer weight ratios. Special attention is given to the pathway of morphological changes.

II. Experimental Section

A. Materials. Monodisperse polystyrene (PS) latex, LS 1102A (Dow Chemical Co.), with 190-nm-diameter particles was used as seed. The PS latex was cleaned by the serum replacement technique until the conductivity of the serum emerging from the filtration cell was close to that of distilled deionized (DDI) water. The monomer, methyl methacrylate (Rohm and Haas Co.), was washed with 10% aqueous sodium hydroxide solution, followed by water, dried overnight (at 5 °C) with anhydrous sodium sulfate (100 g/L), and vacuum distilled under dry nitrogen to remove the inhibitor. 2,2-Azobis(isobutyronitrile) initiator (Vazo 64, Du Pont Co.) was recrystallized twice from ethanol and then dried at room temperature in a vacuum oven. All other materials were used as received, including Igepal Co-990 surfactant [nonylphenol poly(ethylene oxide), 100 mol of ethylene oxide; GAF Co.]. Distilled deionized water was used in all polymerizations.

B. Seeded Emulsion Polymerization and Particle Morphology. The composite latexes were prepared by batch-seeded emulsion polymerization by using Dow LS1102A (denoted as PS190) monodisperse polystyrene latex as the seed particles. Methyl methacrylate (MMA) monomer was used in the second-stage polymerization. The seed particles were first swelled by MMA monomer for 1 h and then the second-stage polymerization was carried out at 70 °C in batch using magnetically stirred polymerization bottles. Table II gives the standard recipe used in the preparation of the latex samples PS190/PMMA-AIBN at seed/monomer weight ratios of 50/50 and 65/35. The composite latexes were then cleaned by serum replacement until the refractive index of the serum emerging from the filtration cell was close to the DDI water. The particle morphology was observed by TEM after preferentially staining of the polystyrene domains with RuO_4 vapor and negative staining with phosphotungstic acid (PTA) to better delineate the particle edges, especially for the methacrylate-rich domains, which are unstained by RuO_4[11].

C. Swelling with Solvent. On the basis of the similarity of the thermodynamic properties of toluene and MMA, the composite latex samples of PS190/PMMA-AIBN at 50/50 and 65/35 polymer 1/polymer 2 weight ratios were swelled with toluene at room temperature for 1 week. The volume fraction of swelling agent to polymer was 1/1. The particle morphology was then examined by TEM by two different methods. The first method involved examination of the "dry" latex particle morphology, where a sample of the swollen latex particles was put on a grid and then dried at room temperature to remove the toluene and water. The particle morphology was observed by TEM after preferentially staining of the polystyrene domains with RuO_4 vapor and negative staining with phosphotungstic acid. The second method involved examination of the swollen particle morphology "embedded in ice", where a sample of the swollen particles was frozen by using liquid nitrogen and then examined by TEM.

Table I
Free Energy Changes for Various Morphological Structures of Latex Particles Dispersed in Water[a]

case	$\Delta\psi$ (surface energy/area)	eq no.
A (core–shell)	$F[\gamma_{12}(V_r+1)^{-2/3}+\gamma_{2w}]-\gamma_{1w}Y$	(3)
A″ (inverted core–shell)	$F[\gamma_{12}(V_r^{-1}+1)^{-2/3}+\gamma_{1w}]-\gamma_{1w}Y$	(4)
C (hemisphere 1)	$(F/2)\{(V_r+1)^{-2/3}\gamma_{1w}(1+\cos\theta)+(V_r+1)^{-2/3}(1-\cos\theta)\gamma_{12}+(R_2/R)^2(1+\cos\theta')\gamma_{2w}\}-\gamma_{1w}Y$	(5)
	$(R_2/R)^3=\{1-(V_r+1)^{-1}\{1-(1/8)(1-\cos\theta)[3\sin^2\theta+(1-\cos\theta)^2]\}\}/\{1-(1/8)(1-\cos\theta')[3\sin^2\theta'+(1-\cos\theta')^2]\}$	(6)
	$(R_2/R)=(V_r+1)^{-1/3}\sin\theta/\sin\theta'$	(7)
C″ (hemisphere 2)	$(F/2)\{(R_1/R)^2(1+\cos\theta')\gamma_{1w}+\gamma_{12}(1-\cos\theta)(V_r^{-1}+1)^{-2/3}+(V_r^{-1}+1)^{-2/3}(1+\cos\theta)\gamma_{2w}\}-\gamma_{1w}Y$	(8)
	$(R_1/R)^3=\{1-(V_r^{-1}+1)\{1-(1/8)(1-\cos\theta)[3\sin^2\theta+(1-\cos\theta)^2]\}\}/\{1-(1/8)(1-\cos\theta')[3\sin^2\theta'+(1-\cos\theta')^2]\}$	(9)
	$R_1/R=(V_r^{-1}+1)^{-1/3}\sin\theta/\sin\theta'$	(10)
D (individual particles)	$F(\gamma_{1w}+\gamma_{2w}V_r^{2/3})(V_r+1)^{-2/3}-\gamma_{1w}Y$	(11)

[a] Where $Y=K(V_f+1)^{-2/3}$, $K=(1+W_rd_1/d_{2m})^{2/3}$, $V_f=W_rd_1/d_2$, and $F=[Y^{3/2}+(1-d_2/d_{2m})X/(1+1/V_f)]^{2/3}$. d_1, d_2, and d_{2m} are the densities of polymer 1, polymer 2, and monomer 2, respectively. W_r is the weight ratio of total monomer 2 to polymer 1. X is the polymerization conversion. R_1, R_2, and R are the radii of polymer phase 1, polymer phase 2, and the overall composite particles, respectively. θ or θ' (see Figure 1) are the angles between the line that connects the two centers of the hemispheres and the other line that connects the centers and the three-phase point. γ_{12}, γ_{1w}, and γ_{2w} are interfacial tensions between the two polymer phases, polymer phase 1 and water (containing surfactant, if present), and polymer phase 2 and water (containing surfactant, if present), respectively. A polymer phase is defined as polymer 1 or 2 dissolved in MMA monomer. V_r is the volume ratio of polymer phase 2 to polymer phase 1.

Table II
Recipe for Seeded Emulsion Polymerization for PS190/PMMA-AIBN

ingredients	wt, g
PS seed particles	1.0
Igepal Co-990[a]	0.08
monomer	variable
DDI water	11.0
AIBN	variable[b]

[a] Nonylphenol poly(ethylene oxide), 100 mol of ethylene oxide; GAF Co. [b] AIBN/monomer weight ratio = 2.143×10^{-3}.

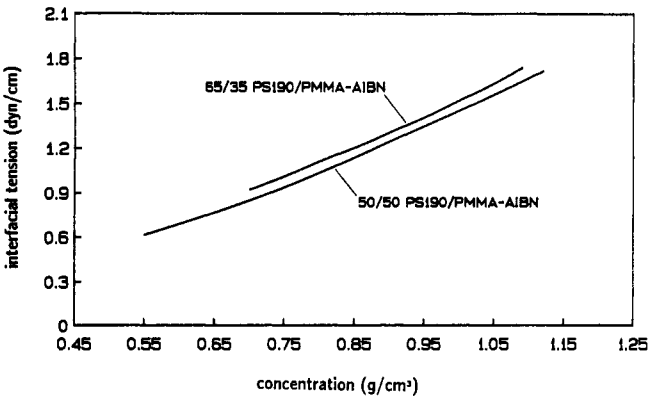

Figure 2. Calculated interfacial tensions of 50/50 and 65/35 weight ratio of polymer 1/polymer 2 system of PS190/PMMA-AIBN as a function of polymer concentration in MMA monomer.

III. Results and Discussion

A. Results of Model Prediction. On the basis of the methodology outlined above and the interfacial tensions reported in our previous work,[13] the composite particle configurations of the PS190/PMMA-AIBN system at weight ratios of 50/50 and 65/35 were predicted by using the equations listed in Table I. The calculation of the free energy change for each case was done by a FORTRAN-77 computer program. The predicted composite particle morphology is the one that has the lowest free energy change.

The required interfacial tensions between polymer phases 1 and 2 and water were determined experimentally by using the drop-weight–volume method.[13] The interfacial tensions between polymer 1 and polymer 2, each dissolved in MMA monomer, were estimated from Figure 2 at the appropriate polymer concentration for PS190/PMMA-AIBN with final weight ratios of 50/50 and 65/35. The interfacial tensions between polymer 1 and polymer 2 as a function of the overall polymer concentration in MMA monomer were calculated on the basis of the work of Broseta et al.[14] They proposed a theory of interfacial tension and concentration profiles for a semidilute solution of two polymers undergoing demixing taking into account the excluded volume effect. In their work they related the interfacial tensions between two polymers undergoing demixing in a semidilute region to the critical concentration of demixing. According to Broseta et al., the interfacial tension can be estimated in terms of measurable quantities such as molecular weight, radius of gyration of chains in the dilute solution, and critical concentration of demixing. Figure 2 gives the calculated results of the interfacial tensions between polymer 1 and polymer 2 as a function of the overall polymer concentration in MMA monomer. This figure simulates the profile of the interfacial tensions as a function of conversion during the course of emulsion polymerization. Figure 2 indicates that the interfacial tension would increase with conversion. Therefore, the tendency of phase separation of polymer phases in the composite latex during the course of seeded emulsion polymerization is also expected to increase.

The last two columns of Table III show the predicted morphology based on thermodynamic calculations and the observed morphology based on TEM examination of the composite particles. For the PS190/PMMA-AIBN system at 50/50 weight ratio, the predicted morphology was case C″ (see Figure 1) with a θ angle of 109°. The electron micrograph given in Figure 3 shows that some particles have a case C″-type morphology, where the polystyrene darker regions are partially covering the PMMA lighter regions (see particle A). This kind of morphology agrees with the theoretical predictions. On the other hand, the electron micrograph also shows that some other particles have a sandwich-like structure (see particle B). This type of morphology could be the result of restricted chain mobility due to high viscosity at the polymerization locus, thus preventing the thermodynamically predicted configuration from being attained. In order to understand how these different composite latex particle morphologies occurred, it is important to study the morphological changes that take place during the course of the polymerization.

Table III shows that the predicted morphology for the 65/35 weight ratio PS190/PMMA-AIBN is case C″, but with a θ angle of 116°. The actual morphology of the composite particles is shown in the transmission electron

Table III
Configurations of PS190/PMMA-AIBN Latex Systems

PS190/PMMA-AIBN weight ratio	V_r[d]	γ_{1w}[a]	γ_{2w}[a]	final configurations: γ_{12}	case predicted		obsd
30/70	2.061	4.46	5.66	1.50[c]	C″	$\theta = 92°$	C″ [c]
50/50	0.883	4.46	5.66	1.55[b]	C″	$\theta = 109°$	C″
65/35	0.476	4.46	5.66	1.63[b]	C″	$\theta = 116°$	C″

[a] Figure 2 in ref 13. Average of at least three measurements, with a precision of ±0.02 dyn/cm. [b] Figure 2, this paper, at 90% conversion (1.05 g/cm^3 on x axis). [c] See ref 13. [d] V_r is the volume ratio of polymer phase 2 to polymer phase 1 at 100% conversion.

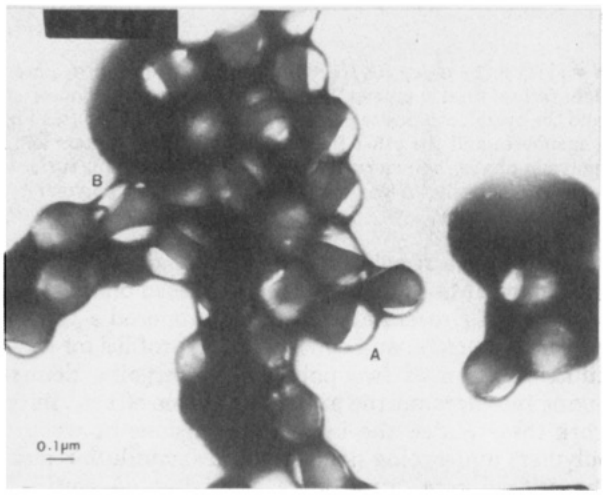

Figure 3. TEM of PS190/PMMA-AIBN composite latex with 50/50 weight ratio. Dark regions are PS domains stained with RuO_4 and lighter regions are PMMA domains outlined by using phosphotungstic acid stain.

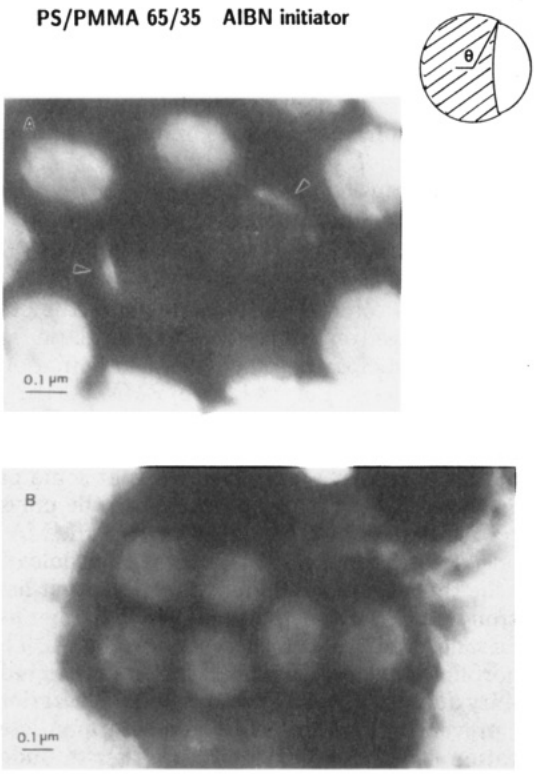

Figure 4. TEM of seed PS190/PMMA-AIBN composite latex with 65/35 weight ratio. Dark regions are PS domains stained with RuO_4 and lighter regions are PMMA domains (arrowhead) outlined by using phosphotungstic acid stain.

micrograph given in Figure 4A, which demonstrates that the second-stage polymer PMMA (lighter region, see arrows) is partially engulfed by the seed polystyrene (darker region). Only a small PMMA domain can be observed. The observed particle morphology corresponds quite well to its schematic representation based on the predicted θ angle in which the polystyrene domain (dashed region) appears as a cap partially covering the PMMA domains. However, in Figure 4B the micrograph also shows that only polystyrene domains can be observed. The explanation for this micrograph is that either the small PMMA domains stick on the sample grid and thus are hidden underneath the PS domains or they are completely engulfed by the seed polystyrene due to the high diffusion resistance, related to restricted chain mobility as a result of the high viscosity at the polymerization locus.

A comparison of the particle morphologies shown in Figures 3 and 4A (both are case C″) demonstrates that the composite latex particles prepared at 65/35 seed/monomer weight ratio [volume ratio (V_r) of polymer 2 to polymer 1, $V_r = 0.476$] have a lower degree of phase separation (higher θ angle; see Table III) than particles prepared at 50/50 polymer weight ratio ($V_r = 0.883$). Further increase in the volume ratio of polymer 2 to polymer 1 ($V_r = 2.061$) for the system of PS seed/MMA monomer weight ratio 30/70 causes further increase in the degree of phase separation as demonstrated by the lowest θ angle of 92° in Table III. The tendency of increasing phase separation with volume ratio of polymer 2 to polymer 1, when $\gamma_{1w} < \gamma_{2w}$, has been predicted previously[13] on the basis of thermodynamic analysis. The results given in Table III and Figures 3 and 4 demonstrate experimentally the predicted tendency of increased phase separation with increased volume ratio of the second-stage polymer to seed polymer particle. In this system of composite particles, γ_{1w} (4.46 dyn/cm) is lower than γ_{2w} (5.66 dyn/cm) due to the use of persulfate initiator in preparing the polystyrene seed particles and AIBN initiator for the second-stage PMMA. The SO_4^- chain end groups are more effective in reducing the interfacial tension than are CN end groups.[13]

B. Thermodynamic Considerations of the Dynamics of Morphology Development. The above thermodynamic treatment was applied to some hypothetical configurations in order to understand the dynamics of morphology development in composite latexes during the course of polymerization. For this purpose, several types of morphologies shown in Figure 5 are considered; these morphologies are usually observed in composite latex systems. In Figure 5, N represents the number of domains, either of polymer 1 or polymer 2, which are separated by the other continuous polymer phase. For example, B2, where N equals 2, means two individual domains of polymer 1 separated by a continuous polymer 2 phase. The morphological sets A and A″ as well as C and C″ given in Figure 1 can be regarded as special cases of the sets BN and B″N or CN and C″N, respectively, in which the number of inclusions N is equal to unity. The sets A and A″ can be regarded as special cases of the sets C and C″, in which the θ angle is equal to 180°. The sets BN and

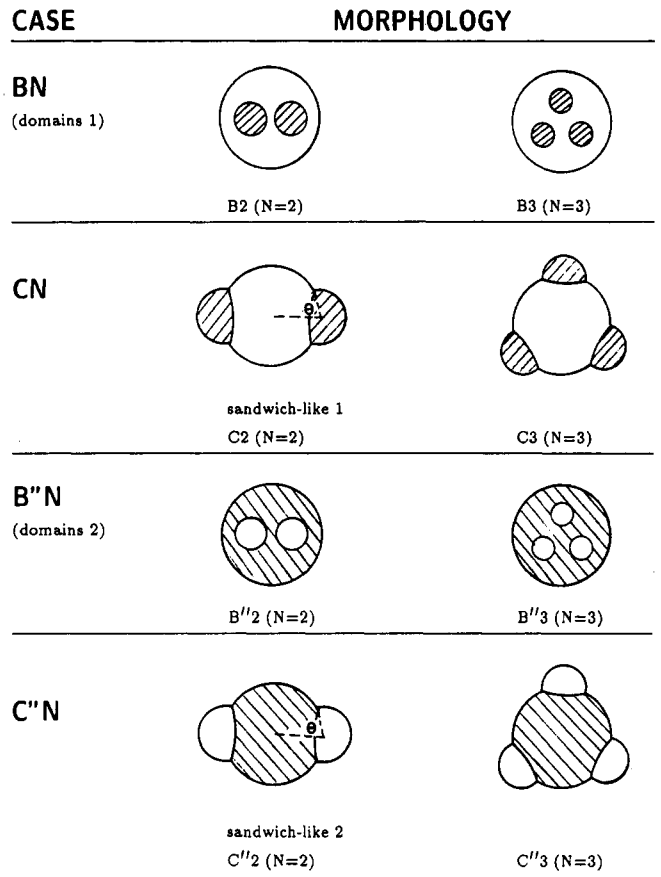

Figure 5. Various morphological structures of particles dispersed in water. ■, polymer 1; □, polymer 2.

B″N can be also regarded as special cases of the sets CN and C″N, in which the θ angle is equal to 180°. The new expressions of the free energy change per unit area, $\Delta\psi$, for the various morphologies given in Figure 5 are summarized in Table IV. Calculations of the free energy changes require knowledge of the interfacial tensions of the two polymers against water as well as between polymer 1 and polymer 2 measured under the prevailing polymerization conditions.

The relative stabilities of each particle morphology case shown in Figures 1 and 5 were determined by calculating the free energy change. The calculation of free energy change involves a trial and error solution method. A FORTRAN77 computer program was developed for that purpose, in which, for a given set of γ_{ij} and V_r data, the values of free energy changes for each case and the thermodynamically preferred morphology were determined. The highest stability of particle morphology is the one that has the lowest free energy change. The polymer/water interfacial tension values, γ_{1w} = 4.46 dyn/cm and γ_{2w} = 5.66 dyn/cm (see Table III), were determined experimentally.[13] The interfacial tensions between the two polymers, γ_{12}, as a function of the overall percent conversion were estimated from Figure 2 at the appropriate overall polymer concentration in MMA; they were found to increase with conversion as shown in Tables V and VI. The distribution of MMA monomer between the two polymer phases was assumed to be proportional to the weight fraction of each polymer. The results of the relative stabilities of morphologies for PS/PMMA-AIBN at 50/50 and 65/35 polymer weight ratios are summarized in Tables V and VI, respectively. The free energy changes for each case in Tables V and VI are plotted in Figures 6 and 7, respectively.

The curves in Figures 6 and 7 show that the free energy change at high conversion is always higher than that at the initial low conversion. This trend is due to the increase in V_r and γ_{12} as the polymer concentration increases with increasing conversion (see Tables V and VI for the values of γ_{12}). Thus, from a thermodynamic point of view, the composite latex particle tends to undergo increased phase separation with increasing conversion during the course of polymerization. However, the extent of achieving the predicted phase separation is controlled by the kinetic aspects of the emulsion polymerization process, which restrict chain mobility.

Analyzing the relative stabilities for cases B″N (or BN) in Tables V or VI and Figure 6 or 7, one finds that the greater the number of inclusions N the less stable the latex morphology. For example, Figures 6 and 7 show that at a given conversion, system B3 (with three inclusions) always displays higher free energy change than B2 (with two inclusions). Thus, the particle morphology with B2 should be relatively more stable than that of B3, provided that no restriction for chain mobility exist. This is because the interface between polymer phases (A_{12}), and therefore $\Delta\psi$, increase with increasing N (see eq 12 or 13 in Table IV). The same conclusions can be applied to cases C″N and CN (see Table V or VI and Figure 6 or 7). For the PS/PMMA-AIBN composite latex system at 50/50 and 65/35 polymer/monomer weight ratios, the most stable particle morphology changes from case A″ to case C″ as the conversion increases (see Tables V and VI). This is due to the increase in polymer 1/polymer 2 interfacial tension as the polymerization proceeds. According to Figure 6, the crossover from structure A″ to C″ as the most stable morphology takes place around 55% conversion for the 50/50 polymer/monomer weight ratio. On the other hand, Figure 7, for the 65/35 polymer/monomer weight ratio, shows that the crossover takes place around 43% conversion.

On the basis of the relative stabilities of the morphologies shown in Table V, several pathways are proposed for particle morphology changes for the 50/50 seed polymer to monomer weight ratio of the PS190/PMMA-AIBN composite latex system during the course of polymerization. For the un-cross-linked polymer systems at hand, particle morphologies with stability levels lower than or equal to case C should not exist under our polymerization conditions (i.e., the reversed morphology in which the polymer with lower interfacial tension against water containing surfactant is engulfed by the polymer with higher interfacial tension against water containing surfactant). These are the morphologies on the right-hand side of the segmental line drawn in Tables V and VI. The possible morphologies at the low conversion of 10% are assumed to be cases A″, C″, B″2, B″3, C″2, and C″3. In the conversion range of 10–40%, the mechanism of morphological changes is shown in Figure 8. This mechanism is based on the premise that all less stable morphologies (with relatively high free energy change) should have a tendency to shift to cases with higher stability (i.e., lower free energy change). Since the rate of morphologic change from one case to the other is dependent on the diffusion resistance (related to the chain mobility), a lower diffusion resistance at the polymerization locus should reduce the probability of finding the less stable morphologies.

As the polymerization progresses further from 40% to 65% conversion, C″ morphology exhibits a higher stability level than A″ morphology, and C″2 is now more stable than B″2. This is shown by the crossover of the corre-

Table IV
Free Energy Changes for Various Morphological Structures of Latex Particles Dispersed in Water[a]

case	$\Delta\psi$ (surface energy/area)	eq no.
BN (domains)	$F[N^{1/3}\gamma_{12}(V_r+1)^{-2/3}+\gamma_{2w}]-\gamma_{1w}Y$	(12)
B″N (domains)	$F[N^{1/3}\gamma_{12}(V_r^{-1}+1)^{-2/3}+\gamma_{1w}]-\gamma_{1w}Y$	(13)
CN	$(F/2)\{(V_r+1)^{-2/3}N^{-1/3}\gamma_{1w}(1+\cos\theta)+(V_r+1)^{-2/3}(1-\cos\theta)N^{1/3}\gamma_{12}+(R_2/R)^2(2-N(1-\cos\theta')\gamma_{2w}\}-\gamma_{1w}Y$	(14)
	$(R_2/R)^3=\{1-(V_r+1)^{-1}[1-(1/8)(1-\cos\theta)[3\sin^2\theta+(1-\cos\theta)^2]]\}/\{1-(N/8)(1-\cos\theta')[3\sin^2\theta'+(1-\cos\theta')^2]\}$	(15)
	$(R_2/R)=[N(V_r+1)]^{-1/3}\sin\theta/\sin\theta'$	(16)
C″N	$(F/2)\{(R_1/R)^2(2-N)(1-\cos\theta')\gamma_{1w}+N^{1/3}\gamma_{12}(1-\cos\theta)(V_r^{-1}+1)^{-2/3}+(V_r^{-1}+1)^{-2/3}(1+\cos\theta)N^{1/3}\gamma_{2w}\}-\gamma_{1w}Y$	(17)
	$(R_1/R)^3=\{1-(V_r^{-1}+1)^{-1}[1-(1/8)(1-\cos\theta)[3\sin^2\theta+(1-\cos\theta)^2]]\}/\{1-(N/8)(1-\cos\theta')[3\sin^2\theta'+(1-\cos\theta')^2]\}$	(18)
	$R_1/R=[N(V_r^{-1}+1)]^{-1/3}\sin\theta/\sin\theta'$	(19)

[a] Where $Y=K(V_f+1)^{-2/3}$, $K=(1+W_rd_1/d_{2m})^{2/3}$, and $V_f=W_rd_1/d_2$. $F=[Y^{3/2}+(1-d_2/d_{2m})X/(1+1/V_f)]^{2/3}$. d_1, d_2, and d_{2m} are the densities of polymer 1, polymer 2, and monomer 2, respectively. W_r is the weight ratio of total monomer 2 to polymer 1. X is the polymerization conversion. R_1 and R_2 are the radii of polymer phase 1 and polymer phase 2, respectively. θ and θ' are the angles between the line that connects the two centers of the hemispheres and the other line that connects the centers and the three-phase point.

Table V
Relative Stabilities of Morphologies for PS/PMMA-AIBN at 50/50 Weight Ratio[a]

		decrease ← $\Delta\psi$ → increase												
conversn, %	γ_{12}	increase ← stability → decrease												
10	0.61	A″	C″	B″2	C″2	B″3	C″3	C	D	C2	C3	A	B2	B3
40	0.9	A″	C″	B″2	C″2	B″3	C″3	C	C2	C3	D	A	B2	B3
65	1.2	C″	A″	C″2	B″2	C″3	B″3	C	C2	C3	D	A	B2	B3
86	1.47	C″	A″	C″2	B″2	C	C″3	B″3	C2	C3	D	A	B2	B3
90	1.56	C″	A″	C″2	B″2	C	C″3	B″3	C2	C3	D	A	B2	B3

[a] γ_{1w} = 4.46 dyn/cm; γ_{2w} = 5.66 dyn/cm.

Table VI
Relative Stabilities of Morphologies for PS/PMMA-AIBN at 65/35 Weight Ratio[a]

		decrease ← $\Delta\psi$ → increase												
conversn, %	γ_{12}	increase ← stability → decrease												
10	0.92	A″	C″	B″2	C″2	B″3	C″3	C	D	C2	C3	A	B2	B3
40	1.15	A″	C″	B″2	C″2	B″3	C″3	C	D	C2	C3	A	B2	B3
50	1.24	C″	A″	C″2	B″2	C″3	B″3	C	C2	D	C3	A	B2	B3
85	1.58	C″	A″	C″2	B″2	C″3	B″3	C	C2	D	C3	A	B2	B3
90	1.63	C″	A″	C″2	B″2	C	C″3	B″3	C2	D	C3	A	B2	B3

[a] γ_{1w} = 4.46 dyn/cm; γ_{2w} = 5.66 dyn/cm.

sponding curves in Figure 6 to lower free energy. Consequently, the new pathways for morphology changes are shown in Figure 9.

The data in Table V show that the relative stabilities of cases C″3 and B″3 decrease during the course of the polymerization. Further increase in conversion from 65% to 86% should cause the disappearance of the less favorable cases C″3 and B″3, with the result of the existence of only four possible morphologies, A″, B″2, C″, and C″2. The morphology change pathways after 86% conversion are indicated in Figure 10; all lead to case C″ as the most stable morphology.

A comparison of the pathways in Figures 8 and 9 for the morphology change between cases B″2 and C″2 shows that, before 40% conversion, composite particles with case C″2 morphology tend to shift to case B″2 morphology. However, after 40% conversion this process is reversed. The change in the morphology from case B″2 to C″2 after 40% conversion may increase the probability of finding particles with case C″2 structure. Indeed, this phenomenon may be responsible for the observed sandwich-like structured particles in the composite particles shown in Figure 3. In addition, analyzing the pathway in Figure 10, one finds that if the diffusion resistance is low enough to allow chain mobility at the site of polymerization, B″2 case should shift to case A″ or C″2 and A″ as well as C″2 cases should shift to case C″. Therefore, only the C″-type morphology should be observed in the final latex. Conversely, if the diffusion resistance is relatively high to restrict chain mobility, the morphologies C″ and C″2 (or A″ and B″2) or a mixture of all four cases (C″, C″2, A″, and B″2) could be observed, depending on how high the diffusion resistance. The result with high diffusion resistance shows a good agreement with the observed particle morphologies in the composite latex system shown in Figure 3. This suggests that a relatively high level of diffusion resistance prevailed during the final stages of the polymerization due to the increased internal particle viscosity.

A similar mechanism of analysis for the particle morphology development can be applied to the PS/PMMA-AIBN system at 65/35 seed polymer to monomer weight ratio. At 10% conversion, Table VI shows that the particles have the following possible morphologies, A″, C″, B″2, C″2, B″3, and C″3. The pathways for particle morphology changes with conversion are similar to those presented in Figures 8–10. In this case, with increasing conversion up to 90% (higher than that for the case of 50/50 polymer/monomer weight ratio) morphologies C″3 and B″3 disappear, and only four possible morphologies, C″, A″, C″2 and B″2, remain viable. The pathways of morphological changes during the final stages of polymerization for conversions higher than 90% are given in Figure 10. If the diffusion resistance would be low, B″2 should shift to A″ or C″2 and A″ as well as C″2 should

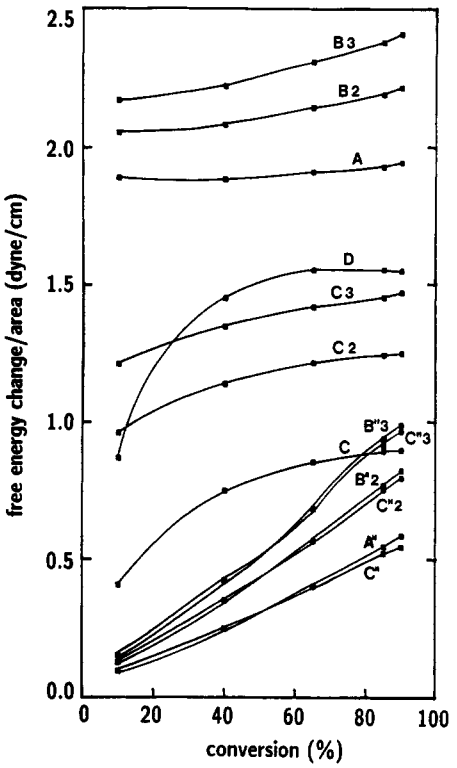

Figure 6. Plot of conversion vs free energy changes for each case in Table V for PS/PMMA-AIBN at 50/50 weight ratio.

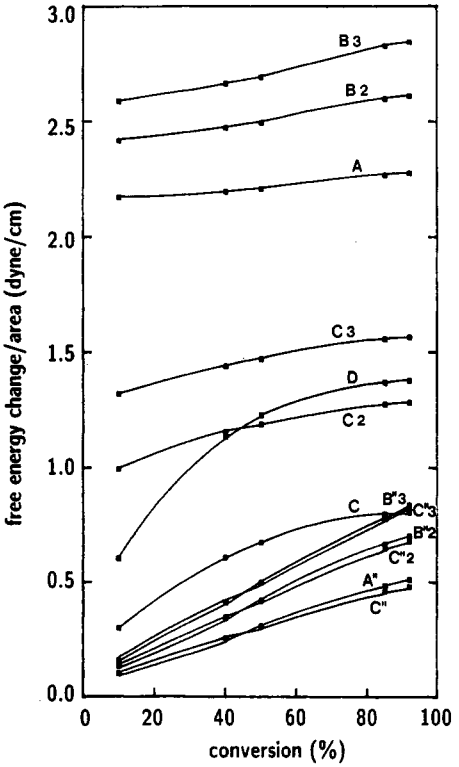

Figure 7. Plot of conversion vs free energy changes for each case in Table VI for PS/PMMA-AIBN at 65/35 weight ratio.

shift to C″, with the result of only C″ morphology to be found in the final latex. However, if the diffusion resistance is dominant, morphologies, C″ and C″2 (or A″ and B″2) or all four cases (C″, A″, C″2, and B″2), may be observed. The TEM particle morphologies presented in Figure 4 for the final composite latex suggest that the diffusion resistance was dominant during the final stage of polymerization, and cases A″ (or B″2) and C″ were the only morphologies observed. The absence of C″2 structure,

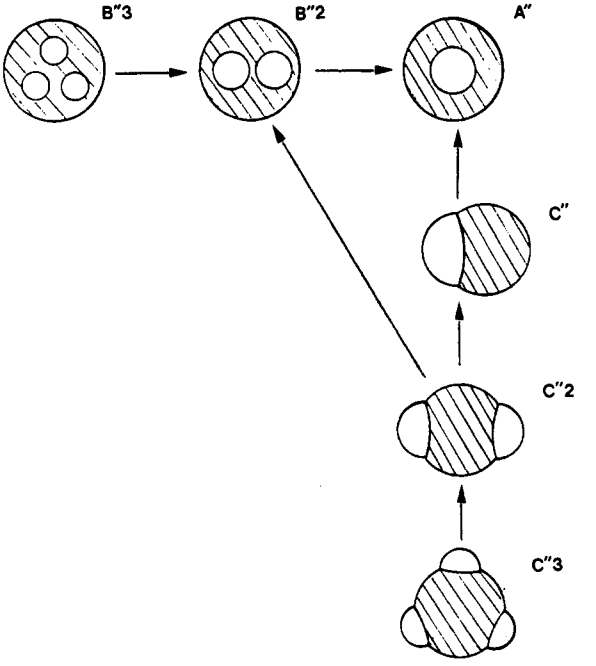

Figure 8. Pathways for various morphological changes in the range of 10–40% conversion during the course of polymerization for 50/50 (or 65/35) weight ratio of seed to monomer. ▨, polymer 1; □, polymer 2.

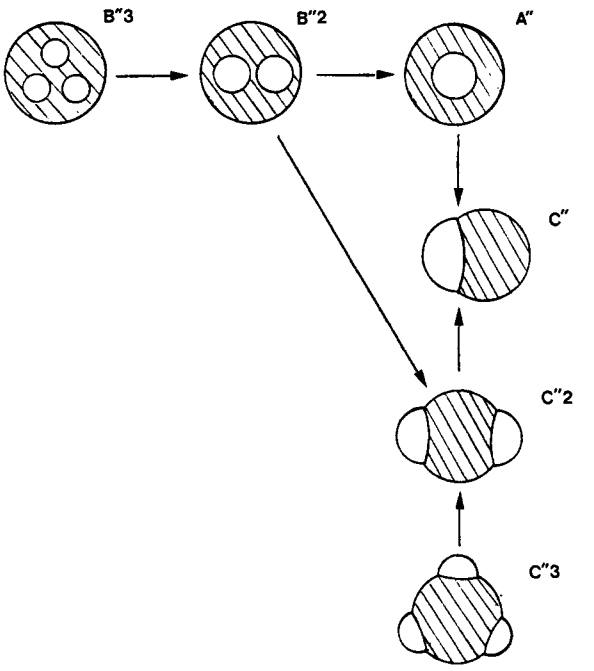

Figure 9. Pathways for various morphological changes in the range of 40–65% (40% to 50%) conversion during the course of polymerization for 50/50 (65/35) weight ratio of seed to monomer. ▨, polymer 1; □, polymer 2.

as compared with the observed particle morphologies in Figure 3, could be due to a higher diffusion resistance. Because of the lower monomer concentration (65/35 seed/monomer weight ratio) used in the preparation of the composite latex and therefore the higher internal viscosity, the possible change in morphology from B″2 to C″2 shown in Figure 9 was hindered.

Confirmation of the above predicted morphological developments during the course of seeded emulsion polymerization requires further experiments to examine the morphology as a function of conversion. This work has not been done yet. However, the above treatment explains

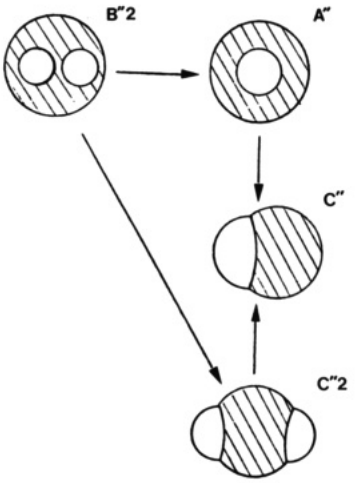

Figure 10. Pathways for various morphological changes after 86% (90%) conversion during the course of polymerization for 50/50 (65/35) weight ratio of seed to monomer. ▨, polymer 1; □, polymer 2.

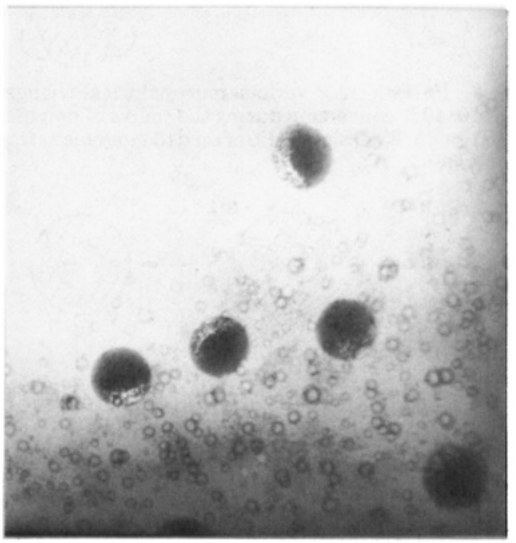

Figure 11. TEM of 50/50 weight ratio PS190/PMMA-AIBN composite latex after treatment with toluene as a swelling agent, "embedded in ice". Lighter regions, PMMA domains, were covered by PS, dark regions.

the possibility of finding more than one morphology in the final composite latex provided that the kinetic factors hinder attainment of the equilibrium morphology. The electron micrographs in Figures 3 and 4 indeed showed that a mixture of particle morphologies exists in the final latex. Postswelling the final composite latex with a solvent was used to examine this point.

C. Swelling with Solvent. Swelling of the final composite particle with a solvent should decrease the internal viscosity and allow chain mobility. This test was utilized in order to demonstrate that by allowing chain mobility the particle morphology with the lowest free energy change, according to Tables V and VI, will prevail. Figure 11 shows the observed particle morphology of composite latex with 50/50 seed polymer to monomer weight ratio of the PS190/PMMA-AIBN system after the final composite latex was swelled with toluene, by the "embedded-in-ice" technique. One can see that the PMMA domains (lighter region) are partially covered by the PS domains (darker region). This result indicates that after swelling with toluene the particle morphology with the lowest free energy change still remained a case C″ structure. The micrographs in Figure 12 show that case

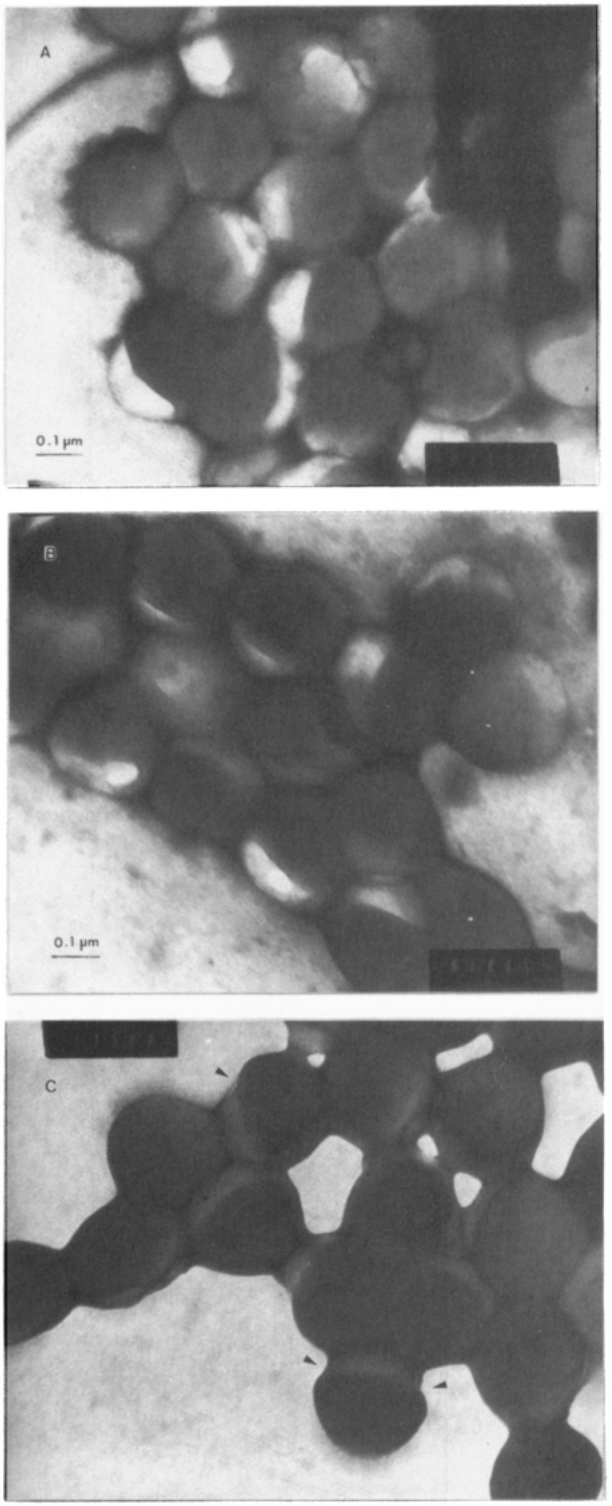

Figure 12. (A, B) TEM of 50/50 weight ratio PS190/PMMA-AIBN "dry" composite latex after treatment with toluene as a swelling agent. Dark regions are PS domains stained with RuO_4 and lighter regions are PMMA domains outlined by using phosphotungstic acid stain. (C) TEM of 50/50 weight ratio PS190/PMMA-AIBN "dry" composite latex after treatment with toluene as a swelling agent (staining with RuO_4 only). As the PMMA was damaged by the electron beam (arrowhead), the cap shape of PS190 was observed.

C″ morphology is also the only morphology seen in the "dry" composite latex of 50/50 seed polymer to monomer weight ratio of the PS190/PMMA-AIBN system after the final composite latex was swelled with toluene. These particles are shown to consist of a PS cap (dark) surrounding a PMMA sphere. Figure 12C clearly shows that as a result of beam damage in the TEM the PMMA

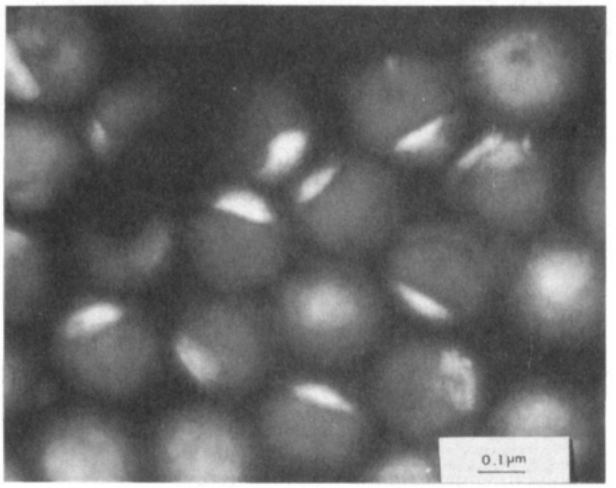

Figure 13. TEM of 65/35 weight ratio PS190/PMMA-AIBN "dry" composite latex after treatment with toluene as a swelling agent. Dark regions are PS domains stained with RuO_4 and lighter regions are PMMA domains outlined by using phosphotungstic acid stain.

domains shrunk (see arrows) and the cap shape of PS domains can be observed. The sandwich-like structures observed in the original composite latex (before swelling with toluene), shown in Figure 3, are no longer observed. This is because the swelling with toluene decreases the diffusion resistance and, therefore, enhances polymer chain mobility so that a thermodynamically more favorable morphology can be achieved. The same phenomenon can be observed in the PS190/PMMA-AIBN system at 65/35 seed polymer to monomer weight ratio. Figure 13 shows that case C″ morphology is the only morphology seen in the composite latex of 65/35 PS190/PMMA-AIBN after swelling with toluene. This should be contrasted with the particle morphology shown in Figure 4, for the original latex before swelling with toluene.

IV. Conclusion

On the basis of experimentally measured interfacial tensions, the proposed pathways of particle morphology changes during the course of seeded emulsion polymerization were derived from a thermodynamic model.

The thermodynamically less stable morphologies should have a tendency to change to structures with higher stability level during the course of polymerization. However, the development of particle morphology is also affected by the diffusion resistance (related to the chain mobility). The increased internal viscosity during the final stage of polymerization causes restricted chain mobility, and as a result, a mixture of particles with more than one morphological configuration is found in the final composite latex. Swelling of the final latex with toluene enhances polymer chain mobility, and thus the thermodynamically more favorable morphology can be achieved.

Acknowledgment. The assistance of Mrs. O. Shaffer with electron microscopy is highly appreciated. We sincerely thank reviewer I for his careful consideration of our original manuscript. His comments led to a significant revision of our paper.

References and Notes

(1) Lee, D. I. In *Emulsion Polymers and Emulsion Polymerization*; Bassett, D. R., Hamielec, A. E., Eds.; *ACS Symp. Ser.* **1981**, *No. 165*, 405.
(2) Min, T. T.; Klein, A.; El-Aasser, M. S.; Vanderhoff, J. W. *J. Polym. Sci., Polym. Chem. Ed.* **1983**, *21*, 2845.
(3) Hourston, D. J.; Satgurunthan, R.; Varman, H. *J. Appl. Polym. Sci.* **1986**, *31*, 1955; **1987**, *33*, 215.
(4) Cho, I.; Lee, K.-W. *J. Appl. Polym. Sci.* **1985**, *30*, 1903.
(5) Muroi, S.; Hashimoto, H.; Hosoi, K. *J. Polym. Sci., Polym. Chem. Ed.* **1984**, *22*, 1365.
(6) Lee, D. I.; Ishikawa, T. *J. Polym. Sci., Polym. Chem. Ed.* **1983**, *21*, 147.
(7) Stutman, D. R.; Klein, A.; El-Aasser, M. S.; Vanderhoff, J. W. *Ind. Eng. Chem. Process Res. Dev.* **1985**, *24*, 404.
(8) Okubo, M.; Katsuta, Y.; Matsumoto, T. *J. Polym. Sci., Polym. Lett. Ed.* **1980**, *18*, 481.
(9) Okubo, M.; Yamada, A.; Matsumoto, T. *J. Polym. Sci., Polym. Chem. Ed.* **1980**, *16*, 3219.
(10) Sundberg, D. C.; Casassa, A. P.; Pantazopoulos, J.; Muscato, M. R. *J. Appl. Polym. Sci.* **1990**, *41*, 1425.
(11) Dimonie, V. L.; El-Aasser, M. S.; Vanderhoff, J. W. *Polym. Mater. Sci. Eng.* **1988**, *58*, 821.
(12) Torza, S.; Mason, S. *J. Colloid Interface Sci.* **1970**, *33*, 67.
(13) Chen, Y. C.; Dimonie, V. L.; El-Aasser, M. S. *J. Appl. Polym. Sci.* **1991**, *42*, 1049.
(14) Broseta, D.; Leibler, L. *J. Chem. Phys.* **1987**, *87*, 7248.
(15) See ref 13, Table 10.

Registry No. PS, 9003-53-6; PMMA, 9011-14-7.